land

MDPI

Article

Interchangeability of Cross-Platform Orthophotographic and LiDAR Data in DeepLabV3+-Based Land Cover Classification Method

Shijun Pan [1,*], Keisuke Yoshida [1,*], Satoshi Nishiyama [1], Takashi Kojima [2] and Yutaro Hashimoto [1]

[1] Graduate School of Environmental and Life Science, Okayama University, 2-1-1, Tsushima-Naka, Kita-ku, Okayama-shi 700-8530, Japan; nishiyama.satoshi@okayama-u.ac.jp (S.N.); pux821yx@s.okayama-u.ac.jp (Y.H.)
[2] TOKEN C. E. E. Consultants Co., Ltd., 1-36-1 Azuma-cho, Omiya-ku, Saitama-shi 330-0841, Japan; kojima-t@tokencon.co.jp
* Correspondence: p4b36znn@s.okayama-u.ac.jp (S.P.); yoshida.k@okayama-u.ac.jp (K.Y.)

Abstract: Riverine environmental information includes important data to collect, and the data collection still requires personnel's field surveys. These on-site tasks still face significant limitations (i.e., hard or danger to entry). In recent years, as one of the efficient approaches for data collection, air-vehicle-based Light Detection and Ranging technologies have already been applied in global environmental research, i.e., land cover classification (LCC) or environmental monitoring. For this study, the authors specifically focused on seven types of LCC (i.e., bamboo, tree, grass, bare ground, water, road, and clutter) that can be parameterized for flood simulation. A validated airborne LiDAR bathymetry system (ALB) and a UAV-borne green LiDAR System (GLS) were applied in this study for cross-platform analysis of LCC. Furthermore, LiDAR data were visualized using high-contrast color scales to improve the accuracy of land cover classification methods through image fusion techniques. If high-resolution aerial imagery is available, then it must be downscaled to match the resolution of low-resolution point clouds. Cross-platform data interchangeability was assessed by comparing the interchangeability, which measures the absolute difference in overall accuracy (OA) or macro-F1 by comparing the cross-platform interchangeability. It is noteworthy that relying solely on aerial photographs is inadequate for achieving precise labeling, particularly under limited sunlight conditions that can lead to misclassification. In such cases, LiDAR plays a crucial role in facilitating target recognition. All the approaches (i.e., low-resolution digital imagery, LiDAR-derived imagery and image fusion) present results of over 0.65 OA and of around 0.6 macro-F1. The authors found that the vegetation (bamboo, tree, grass) and road species have comparatively better performance compared with clutter and bare ground species. Given the stated conditions, differences in the species derived from different years (ALB from year 2017 and GLS from year 2020) are the main reason. Because the identification of clutter species includes all the items except for the relative species in this research, RGB-based features of the clutter species cannot be substituted easily because of the 3-year gap compared with other species. Derived from on-site reconstruction, the bare ground species also has a further color change between ALB and GLS that leads to decreased interchangeability. In the case of individual species, without considering seasons and platforms, image fusion can classify bamboo and trees with higher F1 scores compared to low-resolution digital imagery and LiDAR-derived imagery, which has especially proved the cross-platform interchangeability in the high vegetation types. In recent years, high-resolution photography (UAV), high-precision LiDAR measurement (ALB, GLS), and satellite imagery have been used. LiDAR measurement equipment is expensive, and measurement opportunities are limited. Based on this, it would be desirable if ALB and GLS could be continuously classified by Artificial

Academic Editors: Antonio Miguel Martínez-Graña, Sijing Ye, Shi Shen, Min Zhao and Zhuolin Tao

Received: 6 January 2025
Revised: 17 January 2025
Accepted: 20 January 2025
Published: 21 January 2025

Citation: Pan, S.; Yoshida, K.; Nishiyama, S.; Kojima, T.; Hashimoto, Y. Interchangeability of Cross-Platform Orthophotographic and LiDAR Data in DeepLabV3+ -Based Land Cover Classification Method. *Land* **2025**, *14*, 217. https://doi.org/10.3390/land14020217

Intelligence, and in this study, the authors investigated such data interchangeability. A unique and crucial aspect of this study is exploring the interchangeability of land cover classification models across different LiDAR platforms.

Keywords: airborne LiDAR bathymetry; cross-platform; deep learning; green LiDAR system; riverine land cover classification

1. Introduction

River-related environmental information includes crucial data such as topographic bathymetry and vegetation attributes, which are particularly necessary to develop balanced river management measures addressing issues such as flood control [1–3] and ecosystem management [4–6]. Previously, obtaining such data necessitated field surveys that require personnel to enter the site. More recently, to overcome this limitation (e.g., difficult entry for on-site surveys because of high vegetation density, fast water flows, and lack of professional personnel), digital surface models (DSMs) and digital terrain models (DTMs) have become indispensable tools for representing terrain conditions (e.g., using the height of the highest point in the DSM minus the height of the lowest point in the DTM to infer the height of the land cover) [7–9]. For this study, the authors specifically examined seven types of land cover: bamboo, tree, grass, bare ground, water, road, and clutter. Based on LiDAR technology characteristics, airborne LiDAR bathymetry (ALB) and unmanned aerial vehicle (UAV)-borne green LiDAR systems (GLSs) have already been applied for riverine environment measurements in Japan [10,11]. In accordance with the described measurement results (i.e., DSM minus DTM), classifying the land cover using these results is becoming an important task for river engineering-related research. The main specific advantages/limitations between ALB and GLS are derived from the flight height and measurement point density, i.e., the much larger area for data collection in unit time (ALB is much higher than flight height) or the more detailed laser points per unit voxel (GLS has a higher measurement point density). In this research, the authors attempt to interchange these two platforms' data after normalizing (i.e., resizing into same size) without considering these differences [10,11].

In recent years, several approaches to overcoming land cover classification (LCC) difficulties have been assessed, including decision tree algorithms [12–14], manual setting of thresholds [15–17], and deep learning [18–20]. Considering the time cost of discovering and extracting features of data, deep learning methods, particularly using the atrous convolution module, present some benefits for effective feature finding. Therefore, the DeepLabV3+ model with an atrous convolution module was chosen for this study.

Subsequently, when used along with the DeepLabV3+ model, the high accuracy of LCC production has been proven in an earlier study [20–22]. These studies used orthophotographs with LiDAR data to classify land cover using a DeepLabV3+ model with an additional module for adding a LiDAR dataset with photographs. It also revealed that, because of the similar features, the recognition accuracy of LCC is high (i.e., the averaged overall accuracy is almost 90%) when training. Validation sets were selected from a similar location and period.

However, the study described above was based on the same platform (e.g., training ALB dataset, predicting ALB dataset). For data collected across platforms (i.e., ALB and GLS), the accuracy of training and predicting the same data type and seasonal cross-platform dataset based on the LCC mapping results derived using this operation has not been demonstrated [20,22,23]. And studies focusing on one study site using different platforms in LCC application using AI are rare. So, in this research, the authors attempt to

overcome this research gap. The reason for the lack of similar reference papers is mainly derived from the innovative device application (i.e., GLS) [20] and the requirement for a high flight height (i.e., ALB needs an airplane to fly to around 500 m in height) [22] and multiple measurement periods on the same study site using different platforms (i.e., March, November from 2017 using ALB and March, November from 2020 using GLS for the measurement in the Gion area, the Asahi River, Japan) [20,22,23]. So, the authors herein attempt to explain the innovation of the cross-platform method used in this research and set experiments for proving the necessity of applying the cross-platform method for LCC mapping.

Additionally, mutual prediction of cross-platform LCC to verify interchangeability (i.e., train an ALB dataset, predict a GLS dataset; train a GLS dataset, predict an ALB dataset) is set as a target of this study. Alternatively, instead of using an additional module for accuracy improvement, this study examined the use of another developed method [20,23] to test the interchangeability of the cross-platform dataset on the LCC task by increasing the features using image fusion derived from imagery and LiDAR. Derived from the high-density divided points in the color bar (high contrast color bar) for LiDAR-based visualization, the differences among bare ground, grass and trees can be observed with much greater clarity. To observe the cross-platform effects on LCC in this study to the greatest degree possible, the same resolution and data styles (i.e., digital imagery, LiDAR) of ALB and GLS in mutual prediction were chosen. However, because of the data limitations, instead of using identical seasons, a similar season-related ALB and GLS dataset were selected. The comparisons conducted for this study obtained from cross-platform mutual predictions were able to elucidate cross-platform data features. They indicated a reasonable method to retain robustness using a deep learning method with cross-platform data in LCC mapping production.

After confirming the interchangeability between ALB and GLS, the possibility of training or predicting cross-platform data to map LCC can be proved. Additionally, cross-platform data can be used as an extension of the other. This motivated the authors herein to focus on this topic, i.e., the interchangeability of cross-platform orthophotographic and LiDAR data in land cover classification.

There are several points herein that are innovative compared with other research:

- Multiple season and platform data collection in the same study site;
- Interchangeability-based comparison between ALB and GLS;
- Application of image fusion technology on remote sensing-based LCC;
- If it can be proved, cross-platform interchangeability for both platforms can be a strong point for the practical implications of solving corresponding financial and seasonal issues.

2. Study Site and Methods

2.1. Study Site

Figure 1a–c present our study site, located on the lower Asahi River, a Class I (state-controlled) river in Japan, flowing through Okayama prefecture into the Seto Inland Sea [23]. Throughout this report, the KP value represents the longitudinal distance (kilometer, km) from the targeted river mouth. The riverbed slope is approximately 1:600 [23]. In the targeted reach, the channel width is about 300 m. The targeted domain was 14.6–15.8 KP (GLS), as shown in Figure 1c, for the land cover classification (LCC).

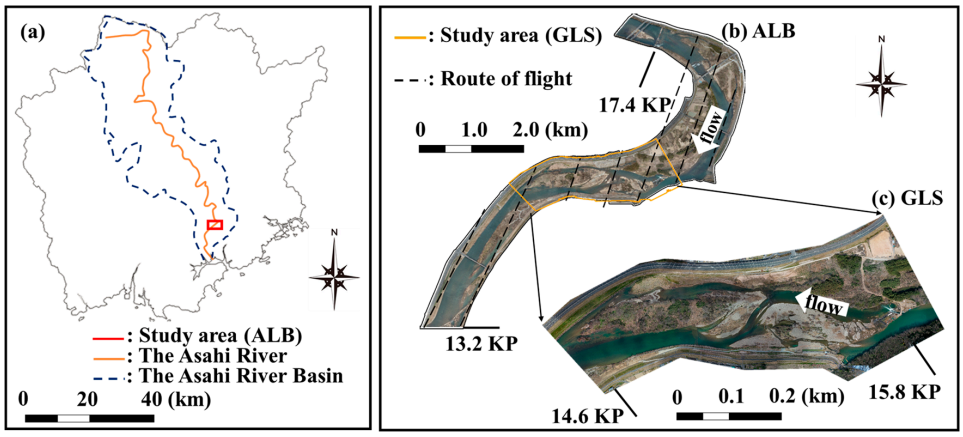

Figure 1. Perspective of airborne LiDAR bathymetry and green LiDAR measurement area: (**a**) location of the Asahi River in Japan with kilo post (KP) values representing longitudinal distance (km) from the river mouth, (**b**) aerial-captured photographs based on the marked positions in (**a**,**c**) drone-captured photographs based on the marked positions in (**b**).

As portrayed in Figure 1c, the GLS part was carried out in the middle of the ALB part. The domain is 1.2 km long, known locally as the "Gion area" (Figure S1 presents details). Consequently, as shown in Figure 2, both ALB and GLS measurements include overland and underwater areas. The LiDAR-based height information extraction process is presented in Figure S2. As shown in Figure S3-1, the land cover species are included in labels.

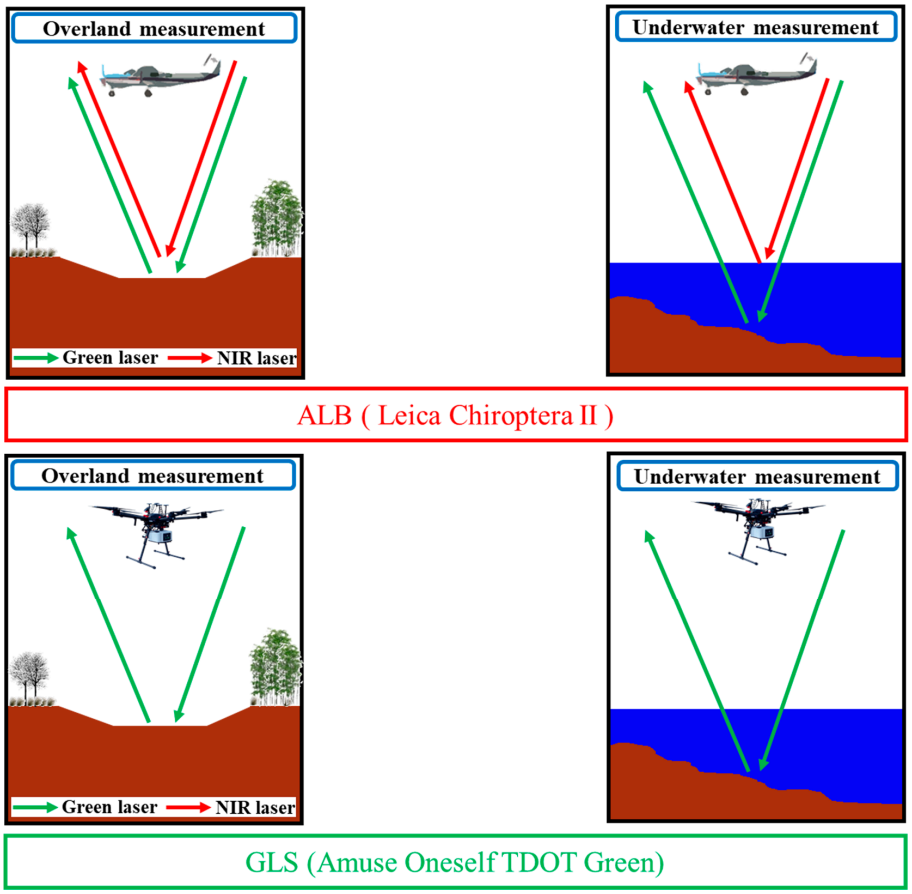

Figure 2. In overland and underwater surveys, Light Detection and Ranging (LiDAR) using near-infrared (NIR) and green laser (GL) from ALB (left side, NIR and GL) and GLS (right-side, GL) is shown, respectively (laser points are shown in grayscale).

Appropriate to its flood control aspects, the riparian vegetation at this study site was classified roughly into three types based on flow resistance characteristics [22,24]: bamboo forests (bamboo), herbaceous species (grass), and woody species (tree). Along with riverine vegetation, this study added another four labels (i.e., water, bare ground, road, and clutter) to better represent local surface environmental changes.

2.2. Workflow

As shown in Figure S4-1, there are mainly 9 steps included in the workflow for proving the cross-platform interchangeability as follows:

1. ALB/GLS: this is a step that use ALB and GLS to collect data;
2. Data processing: a necessary operation for transferring the raw data into usable data for DL;
3. Input data: explaining the data style/species;
4. Processing module: explaining how to process the input data;
5. Data for training/prediction/assessment: separating the processed input data on purpose;
6. DeepLabV3+ module: how to train a DeepLabV3+ model;
7. Trained model: saving the trained model;
8. Prediction: using data for prediction in trained model;
9. Output: using OA and macro-F1 for assessment.

2.3. Data Collection

Based on LiDAR technology characteristics, these years' ALB and GLS have already been applied for riverine environment measurements in Japan, which led to the need for discussing the difference between these two platforms. The main specific advantages/limitations between ALB and GLS are derived from the flight height and measurement point density. In this research, the authors attempt to prove the possibility of cross-platform data.

2.3.1. ALB Part

For this study, we conducted ALB (Leica Chiroptera II; Leica Corp, Wetzlar, Germany) surveys in March and November 2017 along a 4.2 km reach of the lower Asahi River (13.2–17.4 KP), which is controlled by the national government [22]. As shown in Figure 1b, multiple flight operations were conducted in a leaf-off (i.e., March 2017) condition to achieve overlapping coverage of the target area. The current system scanned the river channel for LCC using aircraft-mounted near-infrared (NIR) and green lasers, as presented in Figure 2 [25]. The device commonly uses a green laser to detect underwater (bottom) surfaces because green light can penetrate the water column to some degree. Conversely, the NIR laser is used to detect terrain surfaces, including vegetation, because it is readily reflected by the air–water interface. In the case of ALB, only NIR was used to calculate the vegetation height. Moreover, as shown in Figure 2, a digital camera mounted directly beneath the aircraft took aerial photographs of the target river during each ALB measurement. To remove tilt and relief effects, the aerial photographs were converted to orthophotographs. The aerial photograph overlap and side-lap ratios were, respectively, greater than 60% and 30%. Table 1 presents the equipment specifications, measurement parameters, and river water quality at the time of measurements. The magnitude of turbidity in a river can strongly affect the amount of light incident into the water column. Therefore, its value was confirmed before each ALB measurement. The water quality of the three target periods was reasonable for measuring the underwater terrain surface.

Table 1. Specifications of the present GLS and ALB systems and measurement conditions in the targeted river reach.

Items		ALB 2017		GLS 2020	
		March	**November**	**March**	**October**
Laser wavelength range (nm)	Green	515	515	532	532
	NIR	1064	1064	-	-
Number of laser beams (10^3 s^{-1})	Green	35	35	60	60
	NIR	148	148	-	-
Ground altitude (m)		500	500	50	50
Flight speed (km h^{-1})		220	110	9	9
Measurement point density (m^{-2})	Green	2	4	100	100
	NIR	9.0	9.0	-	-
Resolution of raw imagery (cm $pixel^{-1}$)		10	10	3	3
Resolution of raw LiDAR (m $pixel^{-1}$) *		2	2	1	1
FTU **		-	-	0.8	3.12
NTU ***		-	-	-	3.7
Degree ****		2.9	3.2	-	-

*: Based on LiDAR-I, **: formazin nephelometric unit, ***: nephelometric turbidity unit, ****: one degree of Japan Industrial Standard (JIS K0101) is equivalent to 1 mg of standard substance (kaolin or formazin) contained in 1 L of purified water.

2.3.2. GLS Part

Both the river topo-bathymetry and the vegetation height measurements (i.e., LiDAR data, drone imagery) were performed, respectively, in March and October 2020, with a normal water level using digital drone-mounted GLS [11] through several flight operations. Several water areas lacked measurements in GLS because of low LiDAR power (e.g., density of measurement points) and high turbidity (i.e., caused by low water quality) in the targeted river area. Figure 2 presents a typical view of GLS during overland and underwater measurements. Table 1 shows the equipment specifications related to Figure 2, along with measurement parameters and the river water quality at the time of measurements.

2.4. Data Processing of Imagery-Based Input

Figure 3 depicts the processes for the production of imagery input data for this study. The processing includes four and three types of data for training (LR-TL, LR-DI, LiDAR-I, and image fusion) and for prediction (LR-DI, LiDAR-I, and image fusion), separately: low-resolution true label mapping based on the LiDAR reference derived from high-resolution digital images (LR-TL), low-resolution digital images derived from high-resolution digital images (LR-DI), images derived from LiDAR-based point cloud using a high-contrast color bar (LiDAR-I), and images created by superimposing the above images (image fusion).

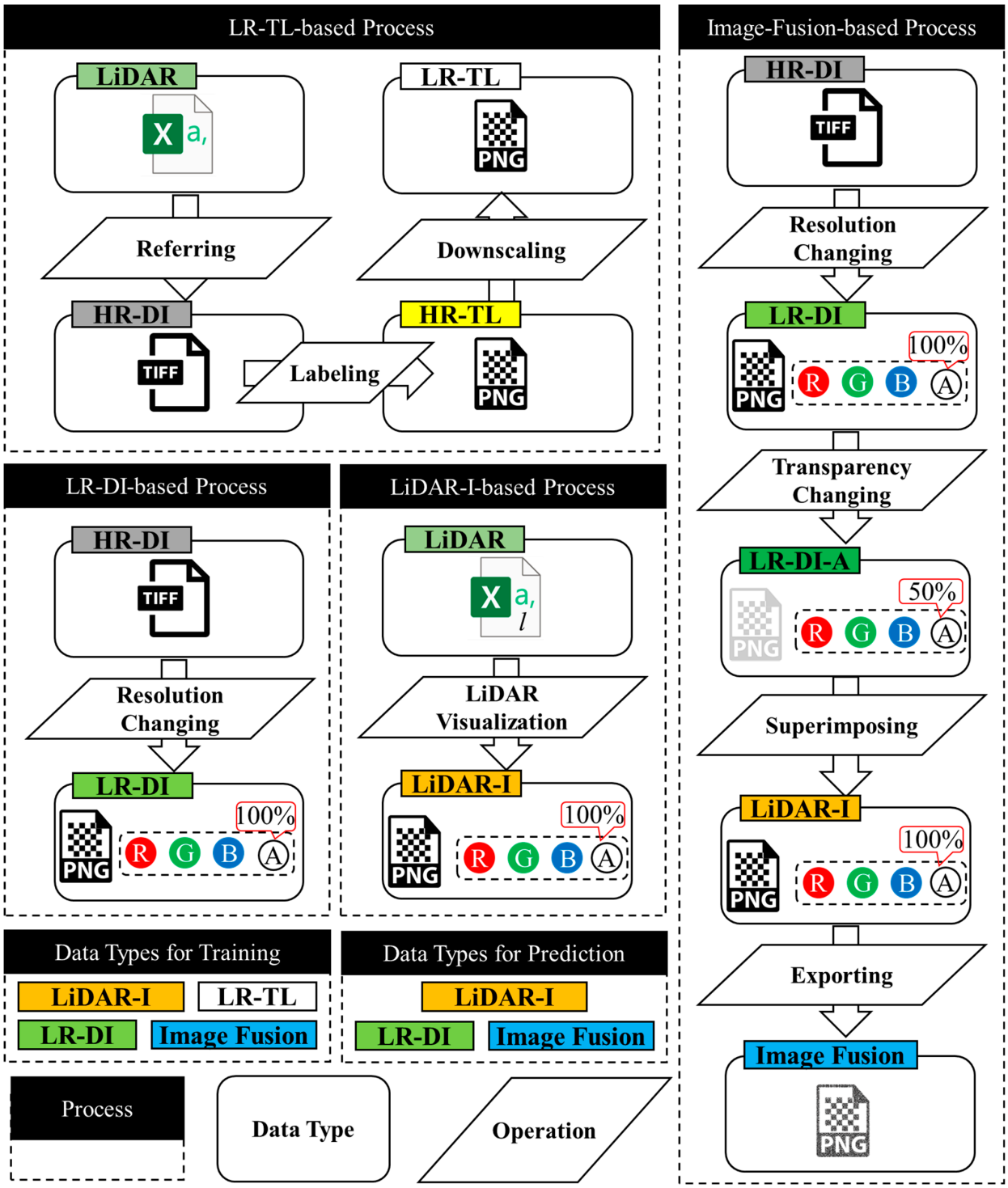

Figure 3. Processes of different data types and responding operations (LR-TL, LR-DI, LiDAR-I, and image fusion).

2.4.1. Preprocessing

When mapping the LCC preprocessing stage, the authors considered earlier field observation experiences [20,22,23] to obtain important assistance for mapping the true label (TL), and this was confirmed by multiple personnel. TL mapping was prepared for assessing the correctness of the predicted LCC mapping. Earlier field observation photographs can provide information about the study target LCC characteristics such as

texture and color difference. Figure S3-1 presents an example of GLS-based TL mapping (i.e., LR-TL) with a close distance.

2.4.2. Transform High-Resolution Imagery to Low-Resolution Imagery (LR-DI)

The resolution conversion operation is necessary to ensure a consistent resolution of these input images. Incidentally, to test the cross-platform interchangeability of several data styles, the 2 m pixel^{-1} resolution was chosen, as shown in Figure S3-2. Resolution transformation in this study uses a non-interpolation approach (i.e., a method that extracts only the color of pixels at fixed intervals) to maintain the color of each pixel in the newly generated image as identical to that of the original image.

2.4.3. Transform LiDAR Data to Imagery (LiDAR-I)

Raw ALB and GLS data include laser point cloud coordinates. As presented in Figure S2, the vegetation height was derived as the height of the highest point in the DSM minus the height of the lowest point in the DTM. To convert the vegetation height information (l) in the csv file into visual imagery, the visualization software Cloud Compare v2.11.1 (Anoia) [64-bit] (i.e., CC, 3-D point cloud and mesh processing software with open source project) was used. Different visualization effects were achieved by changing the types of color scale or the distribution of the selected slider (i.e., the point to set a specific color in the color scale).

Briefly, after comparing the visual effects of various default color scales, the "high-contrast color scale" was chosen for this study. Furthermore, the selected color scale displayed the LiDAR data as imagery after dividing the GLS data (from min to max) into 256 steps. Moreover, the "high-contrast color scale" included six particular slides with different colors in the 0–50% segment of the color scale (i.e., 1%, 2%, 4%, 8%, 16%, and 32%). Derived from the high-density divided points in the 0–50% segment for LiDAR-based visualization, the difference between the familiar land cover (bare ground/grass or tree/grass) can be observed much more clearly than when using the default color bar (Blue > Green > Yellow > Red) in CC.

This color scale was effective for differentiating the laser point cloud better and for characterizing the data better by emphasizing even weakly distinguished image features. Because of the use of multiple split color bands, the "high-contrast color scale" provided better-distinguished data for the l in the first half of the value. Subsequently, the visualized imagery was rendered to files using the zoom-free method. Consequently, the output imagery maintained the same resolution of 1-(GLS) and 2-(ALB) m pixel^{-1}. Eventually, the 1-(GLS) was transformed to 2-(GLS) m pixel^{-1} to maintain the same resolution.

2.4.4. Combine LR-DI with LiDAR-I (Image Fusion)

Because data collection using a single LiDAR sensor remains insufficient, the amount of information for imagery was augmented by integrating data from another sensor, such as a digital camera. Accordingly, the image fusion approach is effective when used with remote sensing to create a fused image that includes clearer, more accurate, and more comprehensive information than from any single image. Actually, image fusion is a combination of two elements: LR-DI and LiDAR-I. As shown in Figure 3, image fusion accomplishes creation and processing using image processing software (i.e., GIMP 2.10.20) with the following steps: 1. Reduce the transparency of the overlay layer to 50%. 2. Maintain the original transparency of the background layer. 3. Merge these two layers into a single image with gamma correction (default method of layer combination in GIMP).

2.5. DeepLabV3+ Model

In earlier studies [11,22], three-channel DeepLabV3+ with an additional module was attempted using a LiDAR dataset as a supplement. In these studies, a four-channel DeepLabV3+ model with a modified input layer was also applied for even higher accuracy. Nevertheless, because of data limitations, it is extremely difficult for the four-channel DeepLabV3+ model to extract features. Therefore, for this study, the authors emphasize the effect of changing the input types and resolution of a cross-platform dataset without changing the internal DeepLabV3+ model. As presented in Figure S4-2, to extract features from input RGB-based imagery (i.e., LR-DI, LiDAR-I, image fusion), the processing of training and inference is represented as the following: 1. trimming raw data from a cross-platform input dataset with a preprocessing module to attain image-based input data (320 pixel × 320 pixel) and then training the input data with a DeepLabV3+ model to achieve a trained model; 2. predicting image-based input data with the trained model, eventually achieving results (i.e., OA and macro-F1 from mutual prediction) [22]; and 3. comparing the averaged and absolute difference values to confirm interchangeability of the cross-platform dataset.

3. Results

3.1. Cross-Platform Interchangeability (With Water Area)

As shown in Figure S3-2, the authors chose the same study site under different seasons (March, October, November), years (2017, 2020) and platforms (ALB, GLS), and all the targeted species (bamboo, tree, grass, bare ground, road, water and clutter) are included. In LiDAR-I, high vegetation (bamboo and tree) and low vegetation (grass) are easy to separate visually, but in LR-DI, without considering the height reference, vegetation-related classifications are difficult. Correspondingly, LR-DI showed its highlighted feature on road and water, and LiDAR-I did not have these feature. After superimposing LiDAR-I and LR-DI as image fusion data, this data type balanced the high stability derived from LiDAR-I and the versatility derived from LR-DI.

As shown in Figure S4-2, three types of 2 m pixel^{-1} input data were used to test interchangeability. As shown in Tables 2 and 3, the following four main comparison parameters were used to quantify interchangeability, i.e., average (OA), average (macro-F1), absolute difference (OA), and absolute difference (macro-F1), which were derived from the six group-based results in Table 4. The overall accuracy (OA) is an accuracy measure reflecting how many of the total pixels are classified correctly. Subsequently, the macro-averaged F1 score (macro-F1) is computed by taking the arithmetic mean (i.e., unweighted mean) of all the per-label F1 scores. Furthermore, a lower absolute difference value (i.e., the difference between training GLS predicting ALB (TGPA) and training ALB predicting GLS (TAPG)) signifies that the cross-platform stability is much better. Figure 4 shows that image fusion has improved in terms of interchangeability, rather than LR-DI and LiDAR-I. Training GLS predicting ALB (TGPA) leads to much higher OA and macro-F1 values using three data styles, separately.

Table 2. Confusion matrix valuation index.

Symbol	Formula
Precision (X) or P.X	TP-X/PR-X
Recall (X) or R.X	TP-X/TL-X
F1 (X)	2 × Precision (X) × Recall (X)/(Precision (X) + Recall (X))
OA	∑ TP-X/Amount of total pixels

Table 2. *Cont.*

Symbol	Formula
Macro-F1	∑ F1 score (X)/Amount of labels

TP-X is the amount of the pixels where true label and prediction are all X. PR-X is the amount of the pixels where prediction is X. TL-X is the amount of the pixels where true label is X.

Table 3. Sample of CM valuation index.

		Prediction									
		C	**R**	**W**	**BG**	**G**	**T**	**B**	**Total**	**Recall**	**F1**
True	C	TP-C	E-C/R	E-C/W	E-C/BG	E-C/G	E-C/T	E-C/B	TL-C	R.C	F1-C
	R	E-R/C	TP-R	E-R/W	E-R/BG	E-R/G	E-R/T	E-R/B	TL-R	R.R	F1-R
	W	E-W/C	E-W/R	TP-W	E-W/BG	E-W/G	E-W/T	E-W/B	TL-W	R.W	F1-W
	BG	E-BG/C	E-BG/R	E-BG/W	TP-BG	E-BG/G	E-BG/T	E-BG/B	TL-BG	R.BG	F1-BG
	G	E-G/C	E-G/R	E-G/W	E-G/BG	TP-G	E-G/T	E-G/B	TL-G	R.G	F1-G
	T	E-T/C	E-T/R	E-T/W	E-T/BG	E-T/G	TP-T	E-T/B	TL-T	R.T	F1-T
	B	E-B/C	E-B/R	E-B/W	E-B/BG	E-B/G	E-B/T	TP-B	TL-B	R.B	F1-B
Total		PR-C	PR-R	PR-W	PR-BG	PR-G	PR-T	PR-B	Total		
Precision		P.C	P.R	P.W	P.BG	P.G	P.T	P.B			

TP-X: amount of the pixels where true label is X. E-X/Y: amount of the pixels where true label is X; prediction is Y.

Table 4. Comparison of 2 m pixel^{-1} resolution cross-platform interchangeability using multiple input styles (LR-DI, LiDAR-I, image fusion) with/without consideration of the water area (GPs, groups).

Data Styles	Groups	Train		Predict		Average (OA)		Average (Macro-F1)	
		GLS	ALB	GLS	ALB	With	Without	With	Without
LR-DI (RGB)	1	○			○	0.73	0.66	0.66	0.62
	2		○	○		0.61	0.62	0.59	0.57
LiDAR-I	3	○			○	0.72	0.61	0.63	0.59
	4		○	○		0.60	0.64	0.56	0.56
Image fusion	5	○			○	0.73	0.63	0.65	0.61
	6		○	○		0.64	0.66	0.60	0.59

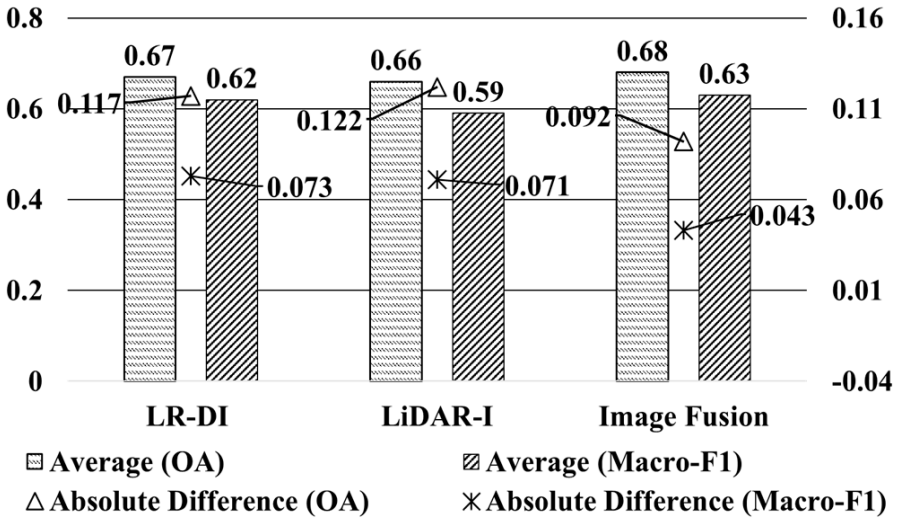

Figure 4. Comparison of data style-based averaged 2 m pixel^{-1} resolution cross-platform interchangeability. Left vertical axis: reference of OA and macro-F1 value; right vertical axis: the reference of absolute difference value.

3.2. Cross-Platform Interchangeability (Without Water Area)

Aside from RGB-only information, the patterns derived from the distribution of the different colors are also extremely important for feature extraction. When training ALB predicting GLS (TAPG), the patterns of ALB water areas have no lack of measurements (LOMs), but GLS water areas have some areas for which measurements are inadequate. Oppositely, compared to TAPG, TGPA has both measured and LOM patterns, as shown in Figure 5 in training (the LOM was derived from the unavailable DTM measurement in this area without green laser penetration into the water). Based on the results described above, the authors inferred the reasons for this phenomenon (that TGPA is better TAPG) as follows: lack of measurement-derived patterns in GLS and ALB did not exist with a pattern of this kind. Even using image fusion, the RGB information derived from ALB-based image fusion and GLS-based image fusion is still much too different for each method. Without considering the water area, as shown in Table 4, OA and macro-F1 derived across platforms become much more similar compared to results considering the water area.

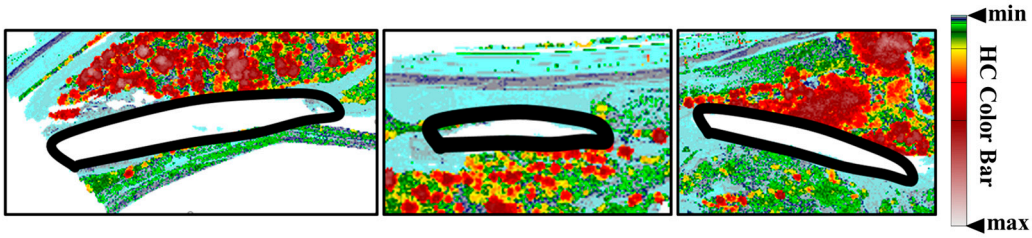

Figure 5. Water areas that are not extractable using GLS alone (i.e., zoom in from LiDAR-I, Oct. 2020). HC means high contrast.

3.3. Cross-Platform Interchangeability (Individual Land Cover)

As the supplement for Table 4, Figure S5 shows the scatter plot of the F1 score on detailed land cover including group 1~6 results without considering the impact of seasons (March, October and November) or data styles (LR-DI, LiDAR-I and image fusion). In Figure S5, the X-axis and Y-axis mean TGPA and TAPG, individually. And all six points of each label have the following meanings:

- X: training all the GLS LR-DI, predicting ALB March 2017 LR-DI. Y: training all the ALB LR-DI, predicting GLS March 2020 LR-DI.
- X: training all the GLS LR-DI, predicting ALB November 2017 LR-DI. Y: training all the ALB LR-DI, predicting GLS October 2020 LR-DI;
- X: training all the GLS LiDAR-I, predicting ALB March 2017 LiDAR-I. Y: training all the ALB LiDAR-I, predicting GLS March 2020 LiDAR-I;
- X: training all the GLS LiDAR-I, predicting ALB November 2017 LiDAR-I. Y: training all the ALB LiDAR-I, predicting GLS October 2020 LiDAR-I;
- X: training all the GLS image fusion, predicting ALB March 2017 image fusion. Y: training all the ALB image fusion, predicting GLS March 2020 image fusion;
- X: training all the GLS image fusion, predicting ALB November 2017 image fusion, Y: training all the ALB image fusion, predicting GLS October 2020 image fusion.

As shown in Figure S5, natural items (bamboo, tree, grass, and water) have comparatively higher cross-platform interchangeability compared with artificial items (bare ground and clutter). The reasons for the higher cross-platform interchangeability are as follows: the features derived from the natural items can be used between platforms, i.e., bamboo and tree are always higher than grass with a green (October or November) or gray (March) color. but bare ground and clutter have different features in different periods, which leads to lower cross-platform interchangeability.

3.4. Cross-Platform Interchangeability (Individual Data Type)

Among the data styles (LR-DI, LiDAR-I and image fusion) in this research, as shown in Figure 4, image fusion has shown its advantage compared with the other two types using OA and macro-F1. After comparing all seven types of land cover, as shown in Table S1, bamboo and tree are the only two types of land cover where the image fusion-derived results (F1 score) are always higher than the LR-DI- and LiDAR-I-derived results.

4. Discussion

4.1. Cross-Platform Interchangeability

Interchangeability analysis between the remote sensing platforms reveals crucially important insights into data reliability and processing efficacy. Investigation of three distinct 2 m pixel^{-1} input data types demonstrated that image fusion techniques improve cross-platform compatibility compared to single-source approaches such as LR-DI and LiDAR-I. As shown in Figure S5, insufficient coverage of the water region generated a systematic imbalance in the data, which contributed to the relative benefit of TGPA, even though it performed better in terms of OA and macro-F1 scores for all data types. This limitation highlights the importance of considering the environmental context when selecting a platform because GLS-based green laser penetration is unable to produce DTM data in some extremely muddy water bodies. When water areas were excluded from this investigation, the cross-platform results showed an increase in similarity, suggesting that greater interchangeability would be beneficial for terrestrial applications. These results demonstrate the importance of image fusion techniques for improving cross-platform reliability, but they also underscore the necessity of additional tactics or alternative measurement techniques for water body analysis applications. This comprehensive understanding of platform interchangeability and its limitations enables better decision-making for remote sensing applications, particularly in areas with diverse topographical features.

Derived from Figure S5, the authors found that the vegetation (bamboo, tree, grass) and road species have comparatively better performance compared with the clutter and bare ground species. Differences in the species derived from different years (ALB from year 2017 and GLS from year 2020) are the main reason for this. Because the identification of clutter species includes all items except for the six mentioned species in this research, the RGB-based feature of the clutter species cannot be interchanged easily because of the 3-year gap compared with the other species. Derived from the on-site reconstruction, the bare ground species also has a further color change between ALB and GLS that leads to decreased interchangeability. As shown in Table S1, image fusion can classify bamboo and tree with a higher F1 compared to LR-DI and LiDAR-I without considering seasons and platforms, which especially proved the cross-platform interchangeability of the high vegetation types.

4.2. Computational Resources and Processing Times

The computational resources and processing times are shown in Tables S2 and S3, separately. Based on the current situation, the GPU hardware and processing time still have potential to be improved correspondingly. The rationale for choosing a 2 m pixel resolution is mainly based on the minimum voxel LiDAR resolution between ALB (2 m pixel resolution) and GLS (1 m pixel resolution) and maintains consistency. And, the 2 m pixel resolution is enough for 2-D flood simulations, which just need the approximate species and height of the vegetation in the riverine environment. In terms of practicality, if using a pixel resolution under 1 m, the file size is too large to save. Because this pixel resolution standard is set for the whole Japanese river, the file size should be as small as possible.

4.3. Limitations and Potential Applications

There are still several limitations of this research:

- Limited study sites were chosen. More study sites should be considered to prove the possibility of LCC-based applications derived from cross-platform LiDAR in other study sites, e.g., if the study site does not include all types of land cover, will the results of LCC be affected or not.
- Only two seasons were included in this research. More seasonal data should be considered to prove the possibility of LCC-based applications derived from cross-platform LiDAR, e.g., if the feature of land cover in the other seasons has not been trained, will the results of LCC be affected or not.
- Only the DeepLabV3+ model was applied in this research. Other open source semantic segmentation models (i.e., U-Net, ResNet and SegForm) should also be considered to prove the verity and generalization of the cross-platform LiDAR applied on LCC, i.e., can the other semantic segmentation models improve the current DeepLabV3+-based LCC accuracy or not.

After proving the interchangeability of ALB and GLS, the authors would like to extend the study sites that have a similar LCC to prove the generalizations. And, if possible, the authors would like to use not just an airplane or drone but also add a satellite platform into the interchangeability comparison. We summarize future works and potential applications as follows:

- More study sites are needed for proving the generalization and verity;
- Interchangeability-based comparisons are not just limited between ALB and GLS but could also consider the satellite platform (e.g., promoting global surface water monitoring research with the SWOT satellite, high-resolution mapping of global surface water and its long-term changes).
- The application of image fusion technology on more remote sensing-based LCC.
- And we consider the potential applications of the obtained results in other tasks:
- The obtained results (LCC) derived from this research can be applied to flood control (setting parameters for flood calculation);
- The obtained results (LCC) derived from this research can be used as basic information of the vegetation environment.

5. Conclusions

This study used cross-platform LiDAR (ALB and GLS) and photographs to elucidate the interchangeability between data derived from platforms in terms of performing LCC. Compared with LR-DI and LiDAR-I, the image fusion approach improved the cross-platform LCC performance. All the approaches present results of over 0.65 OA and of around 0.6 macro-F1. In the case of detailed species comparisons, the vegetation (bamboo, tree, grass) and road species have comparatively better performance (over 0.5 F1 score) compared with the clutter and bare ground species. Increased stability in terms of seasonal and platform change is the main reason for this. In other words, to some degree, cross-platform data can be used for mutual inter-prediction. However, although interchangeability between cross-platform datasets has been proved as described herein, additional input data should be considered to achieve a higher OA and macro-F1. It is noteworthy that digital imagery alone is not sufficient for producing TL mapping under multiple weather conditions (i.e., differing degrees of sunlight intensity) because of the sensitivity of the camera sensor to different weather conditions. Under such circumstances, LiDAR is a considerably important source facilitating the recognition of targets. Finally, both ALB and GLS demonstrated the capability of covering the entire targeted area to measure both overland and underwater areas

(despite some lack of measurement patterns in GLS). Compared with the platforms (ALB and GLS) described above, Mobile Mapping Systems (MMSs) [26] or other on-the-ground LiDAR devices (iPhone or Simultaneous Localization and Mapping, SLAM) [27,28] can collect data in few areas.

Supplementary Materials: The following supporting information can be downloaded at: https://www.mdpi.com/article/10.3390/land14020217/s1.

Author Contributions: Conceptualization, S.P. and K.Y.; methodology, S.P. and T.K.; software, S.P., T.K. and K.Y.; validation, S.P., T.K., K.Y. and Y.H.; formal analysis, S.P.; investigation, S.P.; resources, S.P., K.Y. and S.N.; data curation, S.P. and Y.H.; writing—original draft preparation, S.P.; writing—review and editing, K.Y.; visualization, S.P.; supervision, K.Y. and S.N.; project administration, K.Y. and S.N.; funding acquisition, K.Y. All authors have read and agreed to the published version of the manuscript.

Funding: This research was funded by the River Fund of the River Foundation, Japan, project number 2020-5211-051.

Data Availability Statement: Data related to this research can be made available by request from the corresponding author.

Acknowledgments: The authors appreciate the Okayama River Management Office, Chugoku Regional Development Bureau, Ministry of Land, Infrastructure, Transport and Tourism, Japan, for offering the data related to the Asahi River and Hyakken River.

Conflicts of Interest: The author Takashi Kojima was employed by the company TOKEN C.E.E. Consultants Co., Ltd. The author declares that the research was conducted without any commercial or financial relationship that could be construed as potential conflicts of interest.

Abbreviations

AI	Artificial Intelligence
ALB	airborne LiDAR bathymetry
Conv	convolution
CC	Cloud Compare
DCNN	Deep Convolutional Neural Network
DL	deep learning
DSM	digital surface model
DTM	digital terrain model
GLS	green LiDAR system
GPU	Graphics Processing Unit
HC	high contrast
HR-DI	high-resolution digital image
KP	kilo post
LCC	land cover classification
LiDAR	Light Detection and Ranging
LiDAR-I	Light Detection and Ranging-based Image
LR-DI	low-resolution digital image
LR-DI-A 50%	transparency-changed low-resolution digital image
LR-TL	low-resolution true label
MMS	Mobile Mapping System
NIR	near-infrared
OA	overall accuracy
RGB	Red, Green, Blue
SLAM	Simultaneous Localization and Mapping
TAPG training	ALB predicting GLS
TGPA training	GLS predicting ALB
UAV	unmanned aerial vehicle

References

1. Bureš, L.; Sychová, P.; Maca, P.; Roub, R.; Marval, S. River Bathymetry Model Based on Floodplain Topography. *Water* **2019**, *11*, 1287. [CrossRef]
2. Hilldale, R.C.; Raff, D. Assessing the ability of airborne LiDAR to map river bathymetry. *Earth Surf. Process. Landf.* **2008**, *33*, 773–783. [CrossRef]
3. Lefsky, M.A.; Harding, D.; Cohen, W.B.; Parker, G.; Shugart, H.H. Surface Lidar Remote Sensing of Basal Area and Biomass in Deciduous Forests of Eastern Maryland, USA. *Remote Sens. Environ.* **1999**, *67*, 83–98. [CrossRef]
4. Khosrovyan, A. Biodiversity and Ecosystem Services in Rivers. *Water* **2024**, *16*, 2091. [CrossRef]
5. Sendzimir, J.; Schmutz, S. Challenges in riverine ecosystem management. In *Riverine Ecosystem Management: Science for Governing Towards a Sustainable Future*; Springer: Berlin/Heidelberg, Germany, 2018; pp. 1–16. [CrossRef]
6. Opperman, J.J.; Luster, R.; McKenney, B.A.; Roberts, M.; Meadows, A.W. Ecologically functional floodplains: Connectivity, flow regime, and scale 1. *JAWRA J. Am. Water Resour. Assoc.* **2010**, *46*, 211–226. [CrossRef]
7. Meng, X.; Currit, N.; Zhao, K. Ground filtering algorithms for airborne LiDAR data: A review of critical issues. *Remote Sens.* **2010**, *2*, 833–860. [CrossRef]
8. Khosravipour, A.; Skidmore, A.K.; Isenburg, M.; Wang, T.; Hussin, Y.A. Generating pit-free canopy height models from airborne LiDAR. *Photogramm. Eng. Remote Sens.* **2014**, *80*, 863–872. [CrossRef]
9. Chen, Z.; Gao, B.; Devereux, B. State-of-the-Art: DTM Generation Using Airborne LIDAR Data. *Sensors* **2017**, *17*, 150. [CrossRef]
10. Szafarczyk, A.; Toś, C. The use of green laser in LiDAR bathymetry: State of the art and recent advancements. *Sensors* **2023**, *23*, 292. [CrossRef]
11. Islam, M.T.; Yoshida, K.; Nishiyama, S.; Sakai, K. Novel UAV-borne green LiDAR versus traditional airborne LiDAR: A case study to characterize hydraulic and riparian vegetation attributes. In Proceedings of the 39th IAHR World Congress, Granada, Spain, 19–24 June 2022. [CrossRef]
12. Phiri, D.; Simwanda, M.; Nyirenda, V.; Murayama, Y.; Ranagalage, M. Decision Tree Algorithms for Developing Rulesets for Object-Based Land Cover Classification. *ISPRS Int. J. Geo-Inf.* **2020**, *9*, 329. [CrossRef]
13. Tassi, A.; Vizzari, M. Object-Oriented LULC Classification in Google Earth Engine Combining SNIC, GLCM, and Machine Learning Algorithms. *Remote Sens.* **2020**, *12*, 3776. [CrossRef]
14. Basheer, S.; Wang, X.; Farooque, A.A.; Nawaz, R.A.; Liu, K.; Adekanmbi, T.; Liu, S. Comparison of land use land cover classifiers using different satellite imagery and machine learning techniques. *Remote Sens.* **2022**, *14*, 4978. [CrossRef]
15. Yousefi, S.; Mirzaee, S.; Almohamad, H.; Al Dughairi, A.A.; Gomez, C.; Siamian, N.; Alrasheedi, M.; Abdo, H.G. Image classification and land cover mapping using sentinel-2 imagery: Optimization of SVM parameters. *Land* **2022**, *11*, 993. [CrossRef]
16. Nasiri, V.; Deljouei, A.; Moradi, F.; Sadeghi, S.M.M.; Borz, S.A. Land use and land cover mapping using Sentinel-2, Landsat-8 Satellite Images, and Google Earth Engine: A comparison of two composition methods. *Remote Sens.* **2022**, *14*, 1977. [CrossRef]
17. Mahmoud, R.; Hassanin, M.; Al Feel, H.; Badry, R.M. Machine learning-based land use and land cover mapping using multi-spectral satellite imagery: A case study in Egypt. *Sustainability* **2023**, *15*, 9467. [CrossRef]
18. Li, Y.; Yu, J.; Wang, M.; Xie, M.; Xi, L.; Pang, Y.; Hou, C. Research on the Optimization of Multi-Class Land Cover Classification Using Deep Learning with Multispectral Images. *Land* **2024**, *13*, 603. [CrossRef]
19. Chen, Z.; Xu, Y.; Chen, Y. A Framework for Fine-Grained Land-Cover Classification Using 10 m Sentinel-2 Images. *Remote Sens.* **2024**, *16*, 390. [CrossRef]
20. Pan, S.; Yoshida, K.; Kojima, T.; Nishiyama, S. Drone-LiDAR-assisted Image Fusion methodology for Deep Learning-based Land Cover Classification. *Artif. Intell. Data Sci.* **2022**, *3*, 15–25. [CrossRef]
21. Ayhan, B.; Kwan, C. Tree, shrub, and grass classification using only RGB images. *Remote Sens.* **2020**, *12*, 1333. [CrossRef]
22. Yoshida, K.; Pan, S.; Taniguchi, J.; Nishiyama, S.; Kojima, T.; Islam, M.T. Airborne LiDAR-assisted deep learning methodology for riparian land cover classification using aerial photographs and its application for flood modelling. *J. Hydroinformatics* **2022**, *24*, 179–201. [CrossRef]
23. Yoshida, K.; Pan, S.; Nishiyama, S.; Kojima, T. The Interchangeability of the Cross-Platform Data in the Deep Learning-Based Land Cover Classification Methodology. In Proceedings of the 15th International Conference on Hydroinformatics, Beijing, China, 27–30 May 2024; p. 355. [CrossRef]
24. Jumain, M.; Ibrahim, Z.; Ismail, Z.; Entalai, K.; Makhtar, M.R.; Rahman, M.S.A.; Alias, N. Influence of riparian vegetation on flow resistance in mobile bed straight compound channels. *J. Phys. Conf. Ser.* **2018**, *1049*, 012027. [CrossRef]
25. Matikainen, L.; Karila, K.; Hyyppä, J.; Litkey, P.; Puttonen, E.; Ahokas, E. Object-based analysis of multispectral airborne laser scanner data for land cover classification and map updating. *ISPRS J. Photogramm. Remote Sens.* **2017**, *128*, 298–313. [CrossRef]
26. Ji, J.; Wang, W.; Ning, Y.; Bo, H.; Ren, Y. Research on a Matching Method for Vehicle-Borne Laser Point Cloud and Panoramic Images Based on Occlusion Removal. *Remote Sens.* **2024**, *16*, 2531. [CrossRef]

27. Luetzenburg, G.; Kroon, A.; Kjeldsen, K.K.; Splinter, K.D.; Bjørk, A.A. High-resolution topographic surveying and change detection with the iPhone LiDAR. *Nat. Protoc.* **2024**, *19*, 3520–3541. [CrossRef]
28. Jang, E.; Lee, S.J.; Jo, H. A New Multimodal Map Building Method Using Multiple Object Tracking and Gaussian Process Regression. *Remote Sens.* **2024**, *16*, 2622. [CrossRef]